Spatio-temporal monitoring of a bridge based on 3D point clouds - A comparison among several deformation measurement approaches

Jens-André Paffenholz[1], Daniel Wujanz[2]

[1] Geodetic Institute, Leibniz University Hannover, Nienburger Str. 1, 30167 Hannover, Germany, (paffenholz@gih.uni-hannover.de)
[2] technet GmbH, Am Lehnshof 8, 13467 Berlin, Germany, (daniel.wujanz@technet-gmbh.com)

Key words: laser scanning; uncertainty; stochastic modeling; monitoring; deformation; 3D point clouds; structures

ABSTRACT

This contribution deals with the detection of load-induced arch displacements on a bridge by means of 3D point clouds acquired by terrestrial laser scanning (TLS). TLS has proved to be a suitable technique for geodetic monitoring of structures such as bridges as it allows determining object changes with high accuracy in the low millimeter level at high spatio-temporal resolutions. In an interdisciplinary project, which is being conducted with partners from industry and academia, a historic masonry arch bridge over the river Aller near Verden (Lower Saxony, Germany) has been investigated. Data acquisition was carried out using TLS sensors of kind Zoller+Fröhlich (Z+F) Imager 5006/h in periods of a constant load on the bridge. 3D point clouds for different load scenarios ranging from 1 MN up to 6 MN were captured and finally processed.

This study compares three different approaches for deformation measurements based on the captured 3D point clouds. The first approach under investigation is the Multiscale Model to Model Cloud Comparison (M3C2) algorithm. This algorithm establishes point-to-point correspondences between two 3D point clouds and computes stochastic measures based on the surrounding environment. The second approach is termed Araneo. It establishes correspondences between points and planes in line-of-sight. An extended uncertainty budget considers influences provoked by the applied sensor in form of an intensity-based stochastic model, the effect of spatial sampling as well as the datum-dependent impact of (geo-)referencing . Furthermore, a parametric procedure by means of B-spline approximation to estimate the deformation is deployed. This study reveals notable differences in terms of uncertainty budgets, magnitudes of deformation vectors and detected areal amount of deformation.

I. INTRODUCTION

This contribution deals with the detection of load-induced arch displacements on a bridge by means of 3D point clouds acquired by terrestrial laser scanning (TLS). TLS has proved to be a suitable technique for geodetic monitoring of structures such as bridges as it allows determining object changes with high accuracy in the low millimeter level at high spatio-temporal resolutions. The surface-based data acquisition of the TLS sensors provides a 3D point cloud with typically millions of 3D points, intensity information and optional color information. The use of TLS in the scope of geodetic monitoring and geodetic deformation analysis besides the classical point-wise deformation analysis is a highly topical research field, see, e.g., (Wunderlich et al., 2016). There are solved questions and new challenges (Holst and Kuhlmann, 2016) which are mainly related to the surface-based data acquisition and the high point density.

One of the central challenge can be seen in the suitable modeling of the 3D point cloud to obtain object changes, i.e. deformation measurements. (Neuner et al., 2016) give a detailed overview of modeling strategies of 3D point clouds. An initial classification based on the geometric quantity for the determination of deformations is proposed by (Ohlmann-Lauber and Schäfer, 2011). The authors distinguish between methods working on the raw 3D point could (point- and point cloud-based) and methods based on a modeled 3D point cloud (surface-, geometry- and parameter-based) to obtain geometric object changes.

To judge and interpret changes and differences in the context of a geodetic deformation analysis, the uncertainty budget of the sensor next to the (geo-)referencing procedure and its uncertainty has to be taken into account. An approach considering sensor uncertainties, in particular for the distance measurement, is proposed by (Wujanz et al., 2017). (Paffenholz, 2012) gives an overview of (geo-) referencing strategies as well as an efficient direct (geo-)referencing approach.

The spatio-temporal monitoring based on 3D point clouds is shown for instance for infrastructure buildings, like bridges, e.g., (Liebig et al., 2011; Schill and Eichhorn, 2019) and for dams (Eling, 2009) as well as for a radio telescope (Holst et al., 2015).

This contribution is organized as follows: Section II familiarizes the reader with the methodology of three deformation measurement approaches. The object under investigation, a historic masonry arch bridge, is briefly described in Section III. The results of the spatio-

temporal monitoring of the bridge based on 3D point clouds are shown in Section IV. Finally, the comparison among several deformation measurement approaches is concluded in Section V.

II. METHODOLOGY FOR THE CALCULATION OF DEFORMATION MEASUREMENTS BASED ON 3D POINT CLOUDS

This section briefly introduces the methodology for the calculation of deformation measurements based on 3D point clouds. We will focus on three specific approaches:

A) The multiscale model-to-model cloud comparison (M3C2) algorithm, which uses the raw 3D point cloud by setting up point-to-point correspondences for two 3D point clouds. At a first stage, the M3C2 algorithm neglects the full uncertainty budget of the 3D point clouds.

B) The algorithm Araneo, which uses on the one hand the raw 3D point cloud, on the other hand makes use of planes such that correspondences for points and planes in line-of-sight are established. Furthermore, the uncertainty budget of the 3D point cloud is taken into account.

C) A parametric procedure by means of a B-spline approximation of the 3D point clouds. This is a modeling of the 3D point cloud with the option to consider the assigned uncertainty budget and a subsequent calculation of deformation measurements by means of the approximated 3D point clouds.

(Holst et al., 2017) give an overview of further methodologies and approaches to yield differences of 3D point clouds with the focus on its implementation in standard software.

A. *M3C2 algorithm*

The M3C2 algorithm (Lague et al., 2013) establishes point-to-point correspondences between two 3D point clouds.

The starting point of the M3C2 algorithm is the calculation of core points in one of the 3D point clouds, i.e. called reference 3D point cloud. The core points can be all points of the reference 3D point cloud or an equally spaced, subsampled 3D point cloud. Thus, the core points are calculated as the mean of all points of the original 3D point cloud in a predefined radius.

Subsequently, for each core point the normal vector is calculated by means of a plane estimated from points in a predefined radius. Along with the plane estimation, a variance is provided which indicates the local variation of the 3D point cloud. It is noteworthy, that no distinction is possible between a variation resulting from the surface roughness and the uncertainty of the laser scanner. This local variance can be seen as a precision.

Finally, the core points are projected along the normal vector into the reference 3D point cloud and the other 3D point cloud. The difference for both 3D point clouds is indicated by the distance of both projected points.

An implementation of the M3C2 algorithm is provided by the open source freeware Cloud Compare (www.cloudcompare.org). CloudCompare provides next to 3D point cloud to 3D point cloud differences, significant distance changes, the standard deviation of the core points from the plane estimation as well as the density of the core points at the projection scale.

B. *Araneo*

Araneo (Wujanz, 2019) is an algorithm for the determination of statistically significant deformations in 3D point clouds. The algorithm is assembled by a stochastic as well as a deterministic stage. Based on the reference epoch an uncertainty budget is computed that considers the stochastic characteristics of the applied laser scanner (Wujanz et al., 2017; Schmitz et al., 2019), the sampling uncertainty in object space (Wujanz et al., 2016) as well as the datum-dependent influence of the (geo-)referencing procedure. Subsequently, it establishes correspondences between points from the successive epoch and spherically triangulated surfaces (from the reference epoch) in line-of-sight. By this, the given survey configuration is imitated that notably influences the direction of action of the rangefinder noise. A statistical test that uses the computed stochastic as well as the deterministic measures determine whether a significant deformation has occurred or not.

C. *Parametric procedure by means of B-spline approximation*

Free-form curves and surfaces have been used as part of a standard approximation method for 3D point clouds in many engineering disciplines in the past decade. The 3D point clouds are captured, e.g., by laser scanner, which has been found to be a useful observation technique in different geodetic applications such as 3D surface modeling, monitoring and deformation analysis. For example, (Koch, 2009; Harmening and Neuner, 2015; Bureick et al., 2016) modeled the captured 3D point clouds by means of B-splines and Non-uniform rational B-splines (NURBS). In addition, (Bureick et al., 2016; Xu et al., 2018) used B-splines for the monitoring of different structures, such as rails and arches.

However, the determination of the knots in B-spline approximation (known as knot adjustment problem) significantly affects the estimation of the curve and surface. Therefore, in (Bureick et al., 2016; Bureick et al., 2019) different approaches based on Monte Carlo techniques and genetic algorithms are developed. Both approaches show an optimal selection and optimization of knot vectors for curve approximation.

The second important issue for an optimal B-spline approximation is the adequate number of control points, known as model selection. In case of B-spline

surfaces, model selection comprises a suitable choice of the degree of the basis functions as well as the number of control points in two different directions. In many cases, this task is solved by applying an information criterion, like the Akaike information criterion (AIC) or the Bayesian information criterion (BIC). (Harmening and Neuner, 2016) applied structural risk minimization, originating from statistical learning theory to determine the optimal degree and number of control points of B-spline curves. In (Harmening and Neuner, 2017) this approach is extended to B-spline surfaces. (Alkhatib et al., 2018) discuss a statistical evaluation of the B-splines approximation of 3D point clouds.

Briefly summarized is the workflow for the B-spline approximation of a 3D point cloud as follows: (1) pre-processing of the 3D point cloud, (2) model selection and parametrization, (3) knot vector adjustment and (4) estimation of the B-spline surface in a linear Gauss Markov model, see, e.g., (Paffenholz et al., 2018a) for details.

III. The object under investigation

Figure 1. Side view from West of the arch 4 of the historic masonry arch bridge. The whitewashed area indicates the area of the direct influence of the load application. On the bridge: four hydraulic cylinders for the load application (Paffenholz et al., 2018a).

The object under investigation in this case study is a historic masonry arch bridge over the river Aller near Verden (Lower Saxony, Germany). The aim of the experiment was the combination of numerical models and experimental investigations for model calibration (Schacht et al., 2017). An interdisciplinary project team with partners from industry and academia has carried out two load tests with a maximum load of 570 t (!) in March and June 2016. The contributions from researchers of the Geodetic community were the detection of load-induced arch displacements by means of, e.g., laser scanner, laser tracker and ground based synthetic aperture radar, which is discussed, e.g., in (Paffenholz et al., 2018a; Paffenholz et al., 2018b; Wujanz et al., 2018).

The 3D point cloud acquisition was carried out using TLS sensors of kind Zoller+Fröhlich (Z+F) Imager 5006/h in periods of a constant load on the bridge. 3D point clouds for different load scenarios ranging from 1 MN up to 6 MN were captured and finally processed.

The historic masonry arch bridge was made of circular brick arches of following dimensions: width $14\,m$, depth $8\,m$ and height $4-6\,m$. Figure 1 shows the side view from West of the arch 4 under investigation.

In the scope of the load testing the standard load of 1.0 MN (100 t) should be clearly excited. By this setup first nonlinear deformations should be detected. According to (Schacht et al., 2017) and the references therein, performed numerical simulations stated that a loading with five-times the standard load has to be realized. Thus, a maximum load of approximately 6.0 MN was defined which will be produced by four hydraulic cylinders. These hydraulic cylinders were mounted on the arch (see Figure 1). Injection piles of length 18 m in depth realized the counteracting force. Threaded rods realize the connection of hydraulic cylinders and injection piles. A detailed description of the bridge structure as well as the design of experiments can be found in (Schacht et al., 2017; Schacht et al., 2018).

IV. Results

In this section are discussed the results for the spatio-temporal monitoring of the historic masonry arch bridge. Before the results obtained for the three methods for the calculation of deformation measurements based on 3D point clouds, introduced in Section II, some preliminary inspections for the 3D point clouds are outlined.

A. *Stability of the laser scanner and 3D point cloud with stochastic model*

An important aspect before the actual measurements in the course of the load test were carried out was the choice of a suitable position of the laser scanner in relation to the arch of the bridge. In particular, the safety of the sensors in the event of a failure of the bridge as a result of the load had to be taken into account. From a technical point of view, an optimal position is achieved when the object surface is measured at the smallest possible angle in relation to the surface normal (Soudarissanane et al., 2011). This results in the optimum position directly below the apex of the bridge, which is not possible for obvious reasons. Finally, the choice regarding sensor location was a compromise between the safety aspect mentioned at the beginning and an optimal angle of impact in the sense described above. Therefore, the Eastern edge of the bridge (near the unloaded area) in the immediate proximity of the new steel bridge was chosen as the position.

The chosen sensor location must also be considered with regard to any geometric changes that occur in the soil as a result of the applied load. Possible unconsidered effects lead to deviations of the laser scanner's local coordinates and orientations, which in turn lead to quasi deformations or a general falsification of the results if neglected.

In order to avoid the aforementioned falsification the 3D point clouds were referenced either based on

artificial targets or based on stable areas using a plane-based approach with the software Scantra 2.0.1.20 (www.technet-gmbh.com). The advantage of the plane-based approach is that no artificial targets are required in the scene. Figure 2 shows an intensity image of the reference epoch. This corresponds to a cylindrical projection of the 3D point cloud around the vertical axis of the laser scanner. Stable areas in the area of the new steel bridge were manually selected for referencing. For the referencing of the load epoch into the coordinate system of the reference epoch, up to 870 identical planes were used (see green areas in Figure 2). The standard deviation of the translational components was approx. 0.1 mm, that of the rotations approx. 0.34 milli degrees.

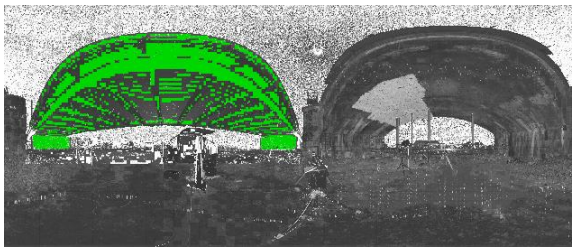

Figure 2. Intensity image of the 3D point cloud with the used planes (green) for the referencing (Wujanz et al., 2018).

In addition to the quality of referencing, the precision of the observations has a decisive influence on the order of magnitude above which deformations can be detected. Using an intensity-based stochastic model according to (Wujanz et al., 2017), the spatial precision σ_{xyz} (standard deviation of a 3D coordinate, Helmert's point error) was calculated for each point of the 3D point cloud. Figure 3 shows a visualization of the 3D point cloud with its stochastic properties in accuracy classes according to (Timmen, 2016). Due to a very heterogeneous distribution of the radiometric properties at the underside of the bridge -from whitewashed surfaces to dark, wet or mossy stones- a strongly varying distribution of the 3D precision results, which is due to the received signal strength. In short: the weaker the signal, the higher the measurement noise.

The range of standard deviations is from about $0.5\,mm$ to $3.0\,mm$. In the dark green colored, rectangular area, the masonry was colored white for photogrammetric measurement. Consequently, the precision of these points stands out from the somewhat more noisy points in the neighborhood. Overall, a decrease in precision can be seen from the upper to the lower areas. This can be explained by flattening incidence angles, which result in a stronger reduction of the intensity. All areas of the arch that are important for the load test fall into the blue to light green range and thus represent a $\sigma_{xyz} \leq 2.4\,mm$. Since the deformations of the bridge are to be expected as a result of the loads in the upper ten millimeter range, it can be concluded that both the precision of the referencing achieved and the precision of the individual measured values are suitable for statistically significant proof of the respective deformations.

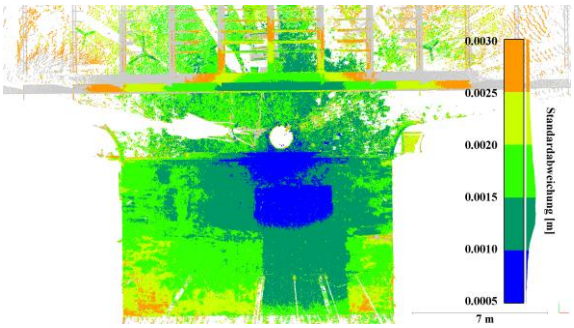

Figure 3. Top view of the 3D point cloud colored by standard deviations. The upper part shows the steel construction of the new bridge, the lower part shows the historic masonry arch bridge (Paffenholz et al., 2018a).

B. *3D point cloud pre-processing*

The acquisition of the 3D point clouds was carried out from a fixed laser scanner position for the various load steps. To support the subsequent calculation and interpretation of deformation measurements, it is worthwhile to perform a 3D point cloud filtering with respect to objects on the arch surface.

Interfering objects which most likely appear differently in various load steps should be carefully removed from the 3D point clouds. These interfering objects are for instance other sensor installations like prisms for the laser tracker and strain gauges. Previous investigations have shown, that aforementioned objects appear differently in the load steps and thus could lead to misinterpretations in the subtraction of a load step with respect to a reference epoch, see (Paffenholz et al., 2018a, Table 2).

C. *M3C2*

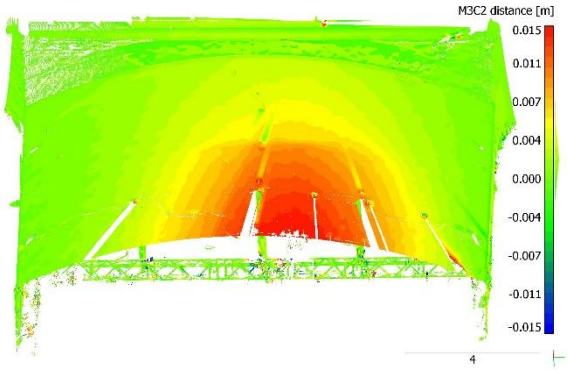

Figure 4. 3D point cloud to 3D point cloud differences (M3C2) for the load scenario of 5 MN. Clearly visible is an arch displacement of up to 14 mm (Paffenholz et al., 2018a).

Figure 4 shows the M3C2 differences for load scenario of 5 MN in a 32-fold graduated color scale of ±15 mm. The maximum arch displacement here is 14 mm in the immediate vicinity of the threaded rods of the load application in the area of the apex of the

arch. The decrease of the deformation in the direction of the pillars and in the direction of the East (upwards in Figure 4) to the unloaded area of the supporting structure is clearly visible.

D. *Araneo*

While Figure 3 already illustrated effects provoked by the applied laser scanner's rangefinder, this section analyzes the influence that is caused by the survey configuration as well as the sampling uncertainty. In Section IV-A), it was mentioned that the laser scanner could not be placed directly underneath the bridge's arch due to the likely event of failure. Nevertheless, the impact that is caused by the survey configuration and the variability of local sampling is of interest. Therefore a 3D point cloud that was captured before the load test served as input. The results are then compared to a 3D point cloud which was captured next to the bridge. In order to avoid overlay of different influences Araneo was used to simulate five different point samplings based on the two input 3D point clouds assuming an error free rangefinder.

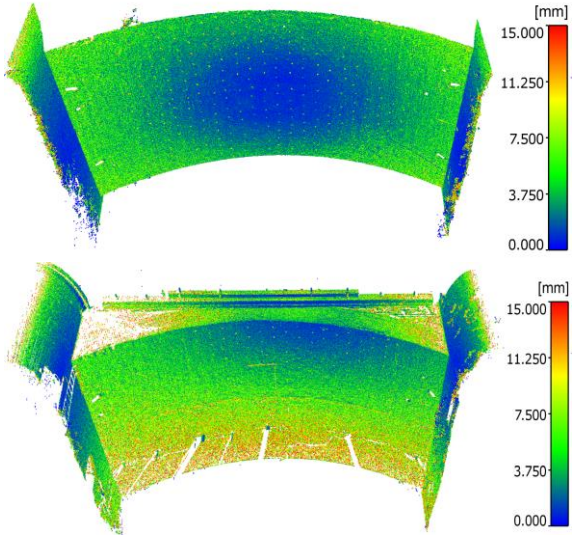

Figure 5. Uncertainty of sampling : 3D point cloud under the arch (top) as well as a lateral 3D point cloud (bottom) (Wujanz, 2019).

The results of this experiment yield in the sampling uncertainty that are depicted in Figure 5. In Figure 5, top, the 3D point cloud captured from underneath the bridge is illustrated, which describes the preferable survey configuration. The sampling uncertainty lies directly above the laser scanner about $0.9\,mm$, recognizable by the blue surface in the middle of the bridge arch. It can also be seen that the sampling uncertainty at the bridge arch increases radially outwards. Similar effects can be seen on the pillars, but in a weakened form due to the more advantageous angle of incidence.

In Figure 5 bottom, the 3D point cloud is depicted,

which was captured about two meters from the edge of the bridge arch. This can be seen in an asymmetrical expansion of the sampling uncertainty, which increases from approx. $1.1\,mm$ to about $15\,mm$ in the transversal direction of the bridge arch. This effect can be explained by the unfavorable recording configuration, which results in flat angles of incidence in the rear area of the arch and a strongly reduced point resolution. This has the consequence that the sampling uncertainty is of similar magnitude than the expected deformations.

E. *Parametric procedure – B-spline approach*

For the approximation of the 3D point clouds by means of a B-spline surface, we performed some preparatory steps.

Firstly, a buffering is performed to reduce the 3D point cloud in the margin areas with the aim to handle data gaps in the margin areas and improve the B-spline approximation.

Secondly, an initial approximation by means of a projection of the 3D point cloud on a regular grid is performed. This simple gridding approach is justified due to a homogenous curvature of the arch, which is characterized by non-occurring curvature changes. Sophisticated approaches to deal with complex surfaces, like Coons Patches, are discussed by (Harmening and Neuner, 2015).

The grid size is chosen with respect to the dimensions of the 3D point cloud of the arch. Chosen is a size of $9\,m$, i.e., 400 grid cells, perpendicular to the bridge centerline and $14\,m$, i.e., 600 grid cells, in direction of the bridge centerline. This gridding results in nearly quadratic grid cells of size $0.022\,m$ and each cell holds 10 3D points of the 3D point cloud.

Based on the calculated B-spline surfaces, deformations of the individual epochs can be detected. Due to the fact that any point can be calculated for an estimated B-spline surface, the differences between two load scenarios can be easily determined. In this context, the points of the corresponding B-spline surface are calculated for each load scenario in a fixed grid of a given grid width. Thus, for each epoch, the function values of the B-spline surface are available in a grid that is uniform for all load scenarios.

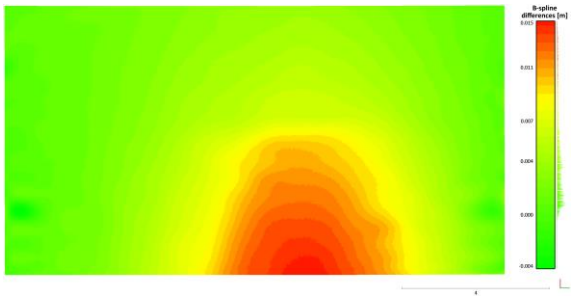

Figure 6. Exemplarily vertical deformation measures for the for the load scenario of 5 MN. The calculations were performed by means of difference for two B-spline surfaces of epoch E00Rw and E55Lw. Clearly visible is an arch displacement of up to 14 mm (Paffenholz et al., 2018a).

In order to calculate the epoch differences between the different load scenarios, only the difference between the uniform grids, i.e. the individual points in the grid cell, of two different epochs has to be calculated. The result is a difference grid, which for each grid cell contains the coordinate differences in all three coordinate directions. The differences in z-direction (vertical deformations) are visualized exemplarily in Figure 6.

V. Conclusion

This study analyzed three different strategies for deformation measurements based on 3D point clouds.

The first approach termed M3C2 establishes correspondences between derived points within a definable proximity. In order to identify significant deformations an error budget is computed that considers measurement noise and (geo-)referencing. Even though this course of action is meaningful, its implementation is subject to simplification.

The second approach named Araneo computes correspondences between points and triangles in accordance to the given survey configuration. Its error budget considers the sampling uncertainty, the stochastic properties of the applied laser scanner as well as the datum-dependent influence of (geo-)referencing.

Just as the M3C2, Araneo identifies deformations for single points whose deterministic signal lies above statistical boundaries.

The last approach follows a parametric strategy and is based on a B-spline approximation of the 3D point cloud. The determination of deformation measurements is based on a difference calculation of two B-spline surfaces. Due to the used gridding approach, this ends up with a calculation of point-wise differences per grid cell. The recent implementation does not consider sensor or (geo-)referencing uncertainties. Their consideration in the stochastic model of the estimation of the B-spline surface in a linear Gauss Markov model is feasible and will be considered in future work.

While comparing the obtained deformation measurements by the M3C2 algorithm (Figure 4) and the B-spline approach (Figure 6), we found no significant difference in the magnitude of vertical displacements. As benefit of the B-spline approach over the M3C2 can be noted that a handling of data gaps due to occlusions in the 3D point clouds is possible.

Even though the results presented in this study were computed under the assumption of equal point precision its stochastic model can and will be assembled with realistic measures which allows to account for sensor characteristics and (geo-)referencing.

References

Alkhatib, H., Kargoll, B., Bureick, J., Paffenholz, J.-A. (2018) Statistical evaluation of the B-splines approximation of 3D point clouds. In: *Proceedings of the XXVI FIG International Congress -Embracing our smart world where the continents connect: enhancing the geospatial maturity of societies-*, available via www.fig.net, Istanbul, Turkey.

Bureick, J., Alkhatib, H., Neumann, I. (2016). Robust Spatial Approximation of Laser Scanner Point Clouds by Means of Free-form Curve Approaches in Deformation Analysis. In: *Journal of Applied Geodesy*, Vol. 10, No. 1, pp. 27–35, doi: 10.1515/jag-2015-0020.

Bureick, J., Alkhatib, H., Neumann, I. (2019). Fast converging elitist genetic algorithm for knot adjustment in B-spline curve approximation. In: *Journal of Applied Geodesy*. (Under review).

Eling, D. (2009). Terrestrisches Laserscanning für die Bauwerksüberwachung. PhD thesis. Munich : DGK (Reihe C, 641).

Harmening, C., Neuner, H. (2015). A constraint-based parameterization technique for B-spline surfaces. In: *Journal of Applied Geodesy*, Vol. 9, No. 3, pp. 143–161, doi: 10.1515/jag-2015-0003.

Harmening, C., Neuner, H. (2016). Choosing the optimal number of B-spline control points. Part 1: Methodology and Approximation of Curves. In: *Journal of Applied Geodesy*, Vol. 10, No. 3, pp. 139–157, doi: 10.1515/jag-2016-0003.

Harmening, C., Neuner, H. (2017). Choosing the optimal number of B-spline control points. Part 2: Approximation of surfaces and applications. In: *Journal of Applied Geodesy*, Vol. 11, No. 1, pp. 43–52, doi: 10.1515/jag-2016-0036.

Holst, C., Nothnagel, A., Blome, M., Becker, P., Eichborn, M., Kuhlmann, H. (2015). Improved area-based deformation analysis of a radio telescope's main reflector based on terrestrial laser scanning. In: *Journal of Applied Geodesy*, Vol. 9, No. 1, pp. 1–14, doi: 10.1515/jag-2014-0018 2015.

Holst, C., Kuhlmann, H. (2016): Challenges and Present Fields of Action at Laser Scanner Based Deformation Analyses. In: *Journal of Applied Geodesy*, Vol. 10, No. 1, pp. 17–25, doi: 10.1515/jag-2015-0025.

Holst, C., Schmitz, B., Schraven, A., Kuhlmann, H. (2017). Eignen sich in Standardsoftware implementierte Punktwolkenvergleiche zur flächenhaften Deformationsanalyse von Bauwerken? Eine Fallstudie anhand von Laserscans einer Holzplatte und einer Staumauer. In: *zfv (Zeitschrift für Geodäsie, Geoinformation und Landmanagement)*, Vol. 142, No. 2, pp. 98–110, doi: 10.12902/zfv-0158-2017.

Koch, K. R. (2009).Fitting free-form surfaces to laserscan data by NURBS, In: *allgemeine vermessungs-nachrichten (avn)*, Vol. 116, No. 4, pp. 134–140.

Lague, D., Brodu, N., Leroux, J. (2013). Accurate 3D comparison of complex topography with terrestrial laser scanner. Application to the Rangitikei canyon (N-Z). In: *ISPRS Journal of Photogrammetry and Remote Sensing*, Vol. 82, pp. 10–26, doi: 10.1016/j.isprsjprs.2013.04.009.

Liebig, J., Grünberg, J., Paffenholz, J.-A., Vennegeerts, H. (2011). Taktile und laserbasierte Messverfahren für die messtechnische Überwachung einer Autobahnbrücke. In: *Bautechnik*, Vol. 88, No. 11, pp. 749–756. doi: 10.1002/bate.201101514 2011.

Neuner, H., Holst, C., Kuhlmann, H. (2016). Overview on current modelling strategies of point clouds for deformation analysis. In: *allgemeine vermessungs-nachrichten (avn)*, Vol. 123, No. 1-12, pp. 328–339.

Ohlmann-Lauber, J., Schäfer, T. (2011). Ansätze zur Ableitung von Deformationen aus TLS-Daten. In: *Terrestrisches Laserscanning - TLS 2011 mit TLS-Challenge*. DVW e.V. (eds.), 106. DVW-Seminar. Augsburg: Wißner-Verlag (Schriftenreihe des DVW, Band 66), pp. 147–157.

Paffenholz, J.-A. (2012). Direct geo-referencing of 3D point clouds with 3D positioning sensors. PhD thesis. Munich : DGK (Reihe C, 689), doi: 10.15488/4698.

Paffenholz, J.-A., Huge, J., Stenz, U. (2018a). Integration of Laser Tracking and Laser Scanning for Optimal Detection of Load Induced Arch Displacement. In: *allgemeine vermessungs-nachrichten (avn)*, Vol. 125, No. 4, pp. 73-88.

Paffenholz, J.-A., Stenz, U., Neumann, I., Dikhoff, I., Riedel, B. (2018b). Belastungsversuche an einer Mauerwerksbrücke: Lasertracking und GBSAR zur Verformungsmessung. In: *Mauerwerk-Kalender 2018.* Jäger, W. (Eds.), Ernst & Sohn: Berlin, pp. 205-219, doi: 10.1002/9783433608050.ch9.

Schacht, G., Piehler, J., Marx, S., Müller, J. (2017). Belastungsversuche an einer historischen Eisenbahn-Gewölbebrücke. In: *Bautechnik*, Vol. 94, No. 2, pp. 125–130, doi: 10.1002/bate.201600084.

Schacht, G., Müller, L., Piehler, J., Meichsner, E., Marx, S. 2018: Belastungsversuche an einer Mauerwerksbrücke: Planung und Vorbereitung der experimentellen Untersuchungen. In: *Mauerwerk-Kalender 2018.* Jäger, W. (Eds.), Ernst & Sohn: Berlin, pp. 93–111, doi: 10.1002/9783433608050.ch5.

Schill, F., Eichhorn, A. (2019). Deformation Monitoring of Railway Bridges with a Profile Laser Scanner. *zfv (Zeitschrift für Geodäsie, Geoinformation und Landmanagement)*, Vol. 144, No. 2, pp. 109-118, doi: 10.12902/zfv-0248-2018.

Schmitz, B., Holst, C., Medic, T., Lichti, D. D., Kuhlmann, H. (2019). How to Efficiently Determine the Range Precision of 3D Terrestrial Laser Scanners. In: *Sensors*, Vol. 19, No. 6, pp. 1466, doi: 10.3390/s19061466.

Soudarissanane, S., Lindenbergh, R., Menenti, M., Teunissen, P. (2011). Scanning geometry: Influencing factor on the quality of terrestrial laser scanning points. In: *ISPRS journal of Photogrammetry and Remote Sensing*, Vol. 66, No. 4, pp. 389-399, doi: 10.1016/j.isprsjprs.2011.01.005.

Timmen, A. (2016). Definition and Derivation of a Quality index for the Visualization of 3D-Point Cloud Quality Parameters in a Virtual Environment. Master thesis (unpublished, in German). Geodetic Institute Hannover, Leibniz University Hannover.

Wujanz, D., Krueger, D., Neitzel, F. (2016). Identification of stable areas in unreferenced laser scans for deformation measurement. In: *The Photogrammetric Record*, Vol. 31, No. 155, pp. 261-280, doi: 10.1111/phor.12152.

Wujanz, D., Burger, M., Mettenleiter, M., Neitzel, F. (2017). An intensity-based stochastic model for terrestrial laser scanners. In: *ISPRS Journal of Photogrammetry and Remote Sensing*, Vol. 125, pp. 146-155, doi: 10.1016/j.isprsjprs.2016.12.006.

Wujanz, D., Burger, M., Neitzel, F., Lichtenberger, R., Schill, F., Eichhorn, A., Stenz, U., Neumann, I., Paffenholz, J.-A. (2018). Belastungsversuche an einer Mauerwerksbrücke: Terrestrisches Laserscanning zur Verformungsmessung. In: *Mauerwerk-Kalender 2018.* Jäger, W. (Eds.), Ernst & Sohn: Berlin, pp. 221-239, doi: 10.1002/9783433608050.ch10.

Wujanz, D. (2019). Araneo: Determination of an Extended Uncertainty Budget for Deformation Measurement Based on Terrestrial Laser Scans. In: *allgemeine vermessungs-nachrichten (avn)*, Vol. 126, No. 3, pp. 53-63.

Wunderlich, T., Niemeier, W., Wujanz, D., Holst, C., Neitzel, F., Kuhlmann, H (2016). Areal deformation analysis from TLS point clouds – the challenge. In: *allgemeine vermessungs-nachrichten (avn)*, Vol. 123, No. 11-12, pp. 340–351.

Xu, X., Kargoll, B., Bureick, J., Yang, H., Alkhatib, H., Neumann, I. (2018). TLS-based profile model analysis of major composite structures with robust B-spline method. In: *Composite Structures*, Vol. 184, pp. 814–820. doi: 10.1016/j.compstruct.2017.10.057.